PCCP

ROYAL SOCIETY OF CHEMISTRY

PAPER

View Article Online
View Journal

Cite this: DOI: 10.1039/d6cp00500d

Strong field ionization and dissociation dynamics of vinyl bromide (C_2H_3Br) initiated by few-cycle pulses

Temitayo A. Olowolafe, Godfred Boakye Adusei, Deep Mukherjee, Andrew S. Durden, Sulaiman Abubakar, Blessed Oguh, Akaninyene Udoikono, Suk Kyoung Lee, H. Bernhard Schlegel and Wen Li *

Received 10th February 2026,
Accepted 26th April 2026

DOI: 10.1039/d6cp00500d

rsc.li/pccp

Photoelectron–photoion (PEPICO) and photoion–photoion (PIPICO) coincidence measurements, coupled with a few-cycle intense laser field, were employed to investigate strong field ionization/dissociation dynamics of vinyl bromide (C_2H_3Br). The angular streaking technique was used to map the recoil-frame angle-dependent ionization rates to identify ionizing orbitals. Dissociative single ionization was mainly attributed to ionizing the lower lying molecular orbitals, suggesting that direct ionization dominates with few-cycle pulses. Three dissociative double ionization channels, both prompt and delayed fragmentation, were identified. Theoretical analysis using time-dependent configuration interaction with complex absorbing potential (TDCI-CAP) and high-level electronic structure methods was performed to elucidate the underlying ionization and dissociation mechanisms.

Introduction

Strong-field ionization (SFI) is a significant tool that allows access to singly and multiply charged molecular ions while enabling real-time probing of coupled electronic and nuclear dynamics. The multiple ionization/dissociation pathways after SFI offer extremely rich dynamical information on various important topics such as nonadiabatic transitions, charge migrations, and coherent control. The employment of coincidence measurement techniques, such as 3D velocity map imaging (VMI)[1,2] and cold target recoil ion momentum spectroscopy (COLTRIMS),[3] has made it possible to study channel-resolved ionization/dissociation dynamics using kinematically complete measurements of all ionic fragments and electrons. One potential complication arising from SFI is the strong coupling between ionization and excitation processes, as the pathway may involve both ionization and post-ionization excitation of ions. This complicates the already complex strong field multi-electron dynamics and requires careful investigation. A good example of such coupling is the pulse duration-dependent dissociation dynamics in methane.[4,5]

A few approaches have been established to disentangle the ionization/dissociation dynamics: (1) the channel-resolved above-threshold ionization (CRATI) approach, in which the ATI comb is measured in coincidence with each fragmentation channel to identify the dominant ionization orbitals based on energetics;[6,7] and (2) angular streaking[8–10] and other related approaches that probe the orbital-dependent asymmetry of SFI.[11,12] In angular streaking, the angle-dependent ionization rate was mapped in the molecular/recoil frame, which can be used to compare with the calculated angle-dependent ionization rate from different orbitals. This method requires the ions to be dissociative[10,13] and has shown strong coupling between ionization and excitation. For example, in CH_3I^+, it was found that a significant amount of CH_3^+ dissociation is produced through first ionizing the HOMO orbital to yield ground state cation and then additional excitation to the dissociative excited state cation.[10] Although these techniques are powerful in disentangling the complex dynamics, strategies that suppress ionization–excitation coupling at the outset are highly desirable, as certain systems may not be suitable to study using the existing methods. One potential solution is to employ ultrashort few-cycle pulses (<5 fs), which can ionize systems but do not allow extended interaction and thus reduce laser-driven coupling between cationic states. Here in this work, we will employ this method to initiate strong field ionization of vinyl bromide. We show that the dissociative states are indeed mainly arising from direct ionization. We further explore the dissociative double ionization pathways and show that both singlet and triplet dicationic states are populated through direct strong field double ionization.

Vinyl bromide (C_2H_3Br) is a prototypical halogenated ethylene with a relatively simple structure, but it has attracted much

Department of Chemistry, Wayne State University, Detroit, MI, 48202, USA.
E-mail: wli@chem.wayne.edu

attention due to its complex dynamics. Previous experimental studies, supported by theoretical calculations, have explored the vibrational spectra of the vinyl bromide cation ($C_2H_3Br^+$) in its ground (X), first excited (A), and second excited (B) electronic states using the mass-analyzed threshold ionization (MATI) method with a combination of nanosecond vacuum ultraviolet (VUV) and UV light sources.[14–17] In strong-field ionization, different conclusions were drawn on which cationic states primarily contribute to C–Br bond breaking in producing the vinyl cation. In an earlier femtosecond XUV transient absorption measurement, the A state was suggested.[18,19] However, a later study indicated that the B state may be the main state leading to C–Br bond dissociation.[20] These observations motivate a more direct experimental characterization of the ionization process initiated by an intense laser field. While angular distributions of ion fragments from intense-field dissociative ionization have been measured,[21,22] and their photodissociation and ionization dynamics have been extensively investigated,[16,18,20,23,24] no molecular/recoil-frame photoelectron angular distribution (RFPAD) measurements under strong-field ionization have been reported to our knowledge. Most importantly, the theoretical prediction of electronic coherence and the presence of ultrafast charge oscillations in the excited states of vinyl bromide cations serve as key motivations to investigate the dynamics in vinyl bromide cations and dications.[24]

Here, we combine coincidence measurements with the angular streaking technique to investigate dissociative single and double-ionization pathways and to obtain the angle-dependent ionization rate of vinyl bromide. Specifically, our results indicate that ionization from the HOMO−2 and HOMO−3 orbitals primarily contributes to the dissociative single-ionization channel. Our photoion–photoion coincidence (PIPICO) map reveals a metastable state in the $CH_3^+ + CBr^+$ channel, as well as prompt dissociation in $CH_3^+ + CBr^+$ and $C_2H_3^+ + Br^+$ channels. High-level calculations were performed to rationalize the dynamics associated with the different ionization pathways.

Experimental methods

A detailed description of our experimental setup has been documented previously.[1,25] Briefly, a few-cycle infrared (IR) pulse was generated using a two-stage amplified Ti:Sapphire laser (KM Labs Red Dragon, 780 nm center wavelength and 1 mJ pulse energy) operating at a 1 kHz repetition rate. The Ti:Sapphire laser system initially produced a 30 fs pulse, which was sent through a 1-m long argon-filled hollow-core fiber (ICON, Imperial College London) to obtain a frequency-broadened spectrum *via* self-phase modulation. The 30 fs pulse duration was measured by the frequency-resolved optical gating (FROG) method. Further compression of the ultrashort pulse to generate few-cycle pulses was achieved with seven pairs of chirped mirrors (Ultrafast Innovations, PC70), which compensated the positive group velocity dispersion (GVD) acquired during propagation through the fiber and various optics. A BK7 wedge was used to fine-tune any residual GVD, and a dispersion scan (D-Scan)[26] technique was employed to characterize the few-cycle pulse, which was measured to be approximately 5 fs.[27,28] A broadband quarter wave plate was inserted to produce an elliptically polarized few-cycle laser pulse with an ellipticity of approximately 0.9. The compressed pulses were then directed into our home-built VMI spectrometer. The VMI detector consisted of two microchannel plates (MCP) in a chevron configuration and a phosphor screen (Photonis, APD). The beam was focused by a concave mirror onto the molecular beam to generate different photofragments with an estimated laser intensity of $\sim 2 \times 10^{14}$ W cm^{-2}. The vinyl bromide sample (98%, Sigma-Aldrich) was introduced into the VMI source chamber through a 20 μm diameter nozzle and was skimmed once before entering the VMI main chamber, in which the beam is intercepted by the laser beam. The produced photofragments were velocity-focused onto the detector, where the PIPICO measurements were performed by digitizing the time-of-flight signal from the MCPs using a high-speed digitizer. For the RFPAD measurements, a photoelectron–photoion coincidence 3D VMI setup with two detectors[29] was employed to measure complete momentum distributions of both ions and electrons in coincidence. This system has been previously described in detail.[10] The RFPAD was obtained by plotting the photoelectron angular distribution (PAD) against a selected ion momentum direction fixed within the polarization plane.

Theoretical methods

The development version of the Gaussian software package[30] was used for all optimization, frequency, TD-DFT, EPT, and EOMCC-IP calculations. OpenMolCAS was used for CASSCF and CASPT2 calculations. Ionization potentials and fragmentation pathways for $C_2H_3Br^+$, and $C_2H_3Br^{2+}$ were calculated at three levels of theory: B3LYP[31,32]/6-311++G(3d,2p),[33] CCSD/cc-pVTZ,[34,35] and CBS-QB3.[36–39] The optimized geometries and harmonic vibrational frequencies were used to calculate the adiabatic enthalpy differences at 0 K for the potential energy surface for dissociative double ionization, shown in Fig. 7. The transition states associated with the dissociation of $C_2H_3Br^{2+}$ to produce $CH_3^+ + CBr^+$ and $C_2H_3^+ + Br^+$ were verified to have a single imaginary vibrational frequency along the reaction coordinate of interest, and IRC calculations confirmed the identity of the reactants and products.[40] Energies for vertical double ionization and excitation were obtained by adding the vertical electronic energy difference for ionization and excitation to the enthalpy of the neutral ground state. Excitation energies of the vinyl bromide cations and dications were calculated with CASSCF,[41] CASPT2,[42] and EOM-IP-CCSD[43] using the cc-pVTZ basis set.

Angle-dependent strong field ionization yields were calculated using time-dependent configuration interaction with complex absorbing potential (TDCI-CAP).[44,45] Simulations were performed with the aug-cc-pVTZ basis set plus a large set of

diffuse functions on each atom (five *s* functions (exponents of 0.0256, 0.0128, 0.0064, 0.0032 and 0.0016), four p functions (exponents of 0.0256, 0.0128, 0.0064 and 0.0032), five d functions (exponents of 0.0512, 0.0256, 0.0128, 0.0064 and 0.0032) and three f functions (exponents of 0.0256, 0.0128 and 0.0064)).[46] The atomic complex absorbing potentials increase from 0 to 10 hartree as a $\sin^2$ function, starting at 3.5× the van der Waals radius and reaching a maximum at 9.5× the van der Waals radius. The molecular absorbing potential is the minimum value of the atomic absorbing potentials. All TDCI simulations were performed using the geometry of the neutral ground state. Angle-dependent strong field ionizations were calculated using a static electric field polarized in the direction of interest; the field is gradually ramped up from zero to a maximum value of E_{max} and then held constant. E_{max} is chosen so that the norm[2] of the wavefunction decreases to about 0.3 by the end of the 19 fs propagation in the direction of greatest ionization.

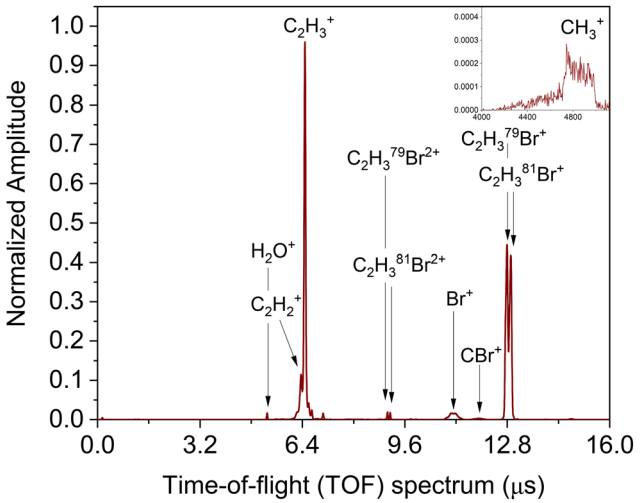

Fig. 1 Time-of-flight spectrum of strong field ionization of vinyl bromide (C_2H_3Br) by few-cycle intense laser pulses. The inset shows the zoomed-in view of the TOF spectrum of CH_3^+.

Results and discussion

Computed ionization potentials

We first calculated the single and double ionization potentials because such data were not systematically available previously. The computed vertical and adiabatic ionization potentials (IPs) are summarized in Table 1. The single and double IPs were obtained using the B3LYP/6-311++G(3d,2p), CCSD/cc-pVTZ, and CBS-QB3 methods. For each process, the three levels of theory agree to within 0.5 eV. The calculated single IPs range from 9.6 to 10.0 eV. The CBS-QB3 adiabatic IP of 9.85 eV agrees very well with the experimental value of 9.8171 ± 0.0006 eV obtained by mass-analyzed threshold ionization (MATI) spectroscopy.[15] Double ionization can yield singlet and triplet dications. The calculated values for vertical ionization range from 27.02 to 27.6 eV. For the triplet, the adiabatic IP is 0.2 lower than the vertical IP, but the difference is 0.95 to 1.1 eV for the singlet dication because of a large change in geometry (see below).

Recoil-frame photoelectron angular distribution (RFPAD) of dissociative single ionization

The ion time-of-flight (TOF) spectrum of SFI of vinyl bromide is shown in Fig. 1. From the spectrum, we see that beside the parent ion ($C_2H_3Br^+$), the vinyl cation ($C_2H_3^+$) is the dominant ion, which arises from dissociative single ionization. This channel has the lowest dissociation energy (see tables in the supplementary information (SI) for the energetics of various channels). Calculations were first carried out to identify the states that lead to the dissociation of the parent ion to $C_2H_3^+$ + Br. The vertical and adiabatic ionization enthalpies for the ground state and first four excited states of vinyl bromide cation (D0–D4) were computed using DFT and TD-DFT with the B3LYP/aug-cc-pVTZ level of theory (Table 2). Each of these five cationic states is well described by a single reference, in which ionization arises with the removal of an electron primarily from a single molecular orbital. Molecular orbitals HOMO to HOMO−4 are shown in Fig. 2. HOMO and HOMO−1 contain nodes in the C–Br bond, and removal of an electron leads to a shorter and stronger bond. HOMO−2 is π bonding, and HOMO−3 is σ bonding in the C-Br region. Removal of an electron from these orbitals leads to C–Br bond elongation and little to no barrier to dissociation. MRCI calculations by Yamaguchi *et al.*[17] showed that there is a barrier of only 0.2–0.3 eV to dissociation from the equilibrium geometry of the D2 state. Since RFPAD probes ionization for dissociative pathways, the measured signal is expected to be dominated by the contributions from HOMO−2 and HOMO−3. This suggests $C_2H_3^+$ is likely produced through ionizing HOMO−2 (D2) and HOMO−3 (D3). But other pathways are also possible: ionizing the HOMO and HOMO−1 orbitals to produce D0 and D1 cationic states

Table 1 Vertical and adiabatic ionization potentials for the vinyl bromide monocation and dication

Ionization potentials (eV)	B3LYP/6-311++G (3d,2p)	CCSD/ cc-pVTZ	CBS-QB3
$C_2H_3Br^+$ D0 vertical	9.73	9.80	10.04
$C_2H_3Br^+$ D0 adiabatic	9.58	9.63	9.85
$C_2H_3Br^{2+}$ S0 vertical	27.25	27.02	27.31
$C_2H_3Br^{2+}$ S0 adiabatic	26.16	26.08	26.36
$C_2H_3Br^{2+}$ T0 vertical	27.19	27.08	27.65
$C_2H_3Br^{2+}$ T0 adiabatic	26.98	26.87	27.42

Table 2 Vertical and adiabatic energies (in eV) of the cationic states of vinyl bromide calculated at the B3LYP/aug-cc-pVTZ level

Cation	Vertical	Adiabatic	Dissociative?
$C_2H_3Br^+$ D0	9.751	9.580	Bound
$C_2H_3Br^+$ D1	10.659	10.614	Bound
$C_2H_3Br^+$ D2	12.487	12.124	Dissociative
$C_2H_3Br^+$ D3	12.689	12.024	Dissociative
$C_2H_3Br^+$ D4	14.839	14.258	Bound

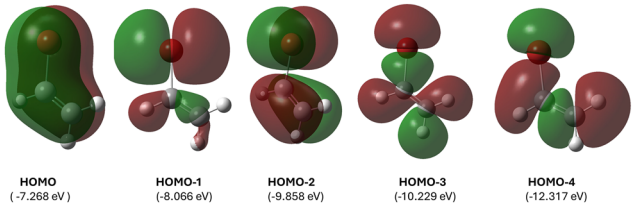

Fig. 2 Relevant molecular orbitals of C_2H_3Br and their energies.

and then absorbing additional photons to reach D2 and D3 states. The D3 state is indeed strongly dipole-coupled to D0.[47] Can the employed few-cycle pulses suppress such pathways? To answer this question, we carried out an angular streaking measurement. The recoil momenta of $C_2H_3^+$ ions and coincident electrons from the dissociative single ionization process were measured, and the RFPAD were produced (Fig. 3a). This was done by rotating the momentum vector of each $C_2H_3^+$ ion to point upward, followed by rotating the coincident electron's momentum vector by the same angle. The image contains 50 000 events. By integrating the electron counts radially at different angles, we obtained the angle-dependent ionization rate for the dissociative channel (Fig. 3b). The technique requires the molecules to dissociate promptly, and thus the rotational motion does not scramble the initial orientation of the molecules (the axial recoil approximation). With the angular streaking principle: the momentum of an emitted electron is rotated ~90 degrees from the initial electric field direction due to the vector potential, we can identify the initial site of ionization. The angle-dependent ionization yield (Fig. 3b) shows a dominant peak from the C_2H_3 side, while the Br side has a smaller peak. Such a clear angle dependence also confirms that the dissociation is largely prompt.

TDCI simulations of the angular dependence of strong field ionization of vinyl bromide were carried out, and the results are shown in Fig. 4. The overall angular dependence is dominated by the HOMO ionization, which shows about equal ionization yields from the vinyl side and the bromine side. This is quite different from what was observed in the experiment. To quantitatively fit the experimental angular dependence, we first extracted the angular dependence of ionization from HOMO−2 and HOMO−3 orbitals as the basis functions, which were obtained by averaging the 3D angle-dependent SFI rates of each orbital about the C–Br bond. We further normalize the angular dependence using the following equation:

$$\eta_{\mathrm{iso}} = \frac{\text{ionization yield} - \min(\text{ionization yield})}{\max(\text{ionization yield}) - \min(\text{ionization yield})}$$

This normalized quantity enhances the angle dependence of ionization by removing the isotropic background, which could arise from partial rotational scrambling in the experiment. We performed such normalization on both the calculated and measured angular dependence of ionization yields. The experimentally observed η_{iso} is compared to the simulated profiles shown in Fig. 5. A linear combination of the three calculated curves (the ground state, excited state 2, and excited state 3) was fitted to the experimental angular dependence. This result shows that HOMO−2 contributes 85% while HOMO−3 contributes ~15% to the total dissociative ionization yield. The flat peak at the vinyl end reflects the characteristic nodal plane in the π-type molecular orbital, while the enhancement of ionization at the Br end indicates the additional contribution of the sigma-type orbital. Adding contributions from HOMO and HOMO−1 ionization does not improve the overall fitting. Therefore, we can conclude that with the few-cycle pulse excitation, the SFI dynamics are limited to direct ionization of molecular orbitals.

Resolving dissociative double ionization pathways

We now move to discuss the double ionization dynamics of vinyl bromide, and we will focus on the dissociation pathways. From the TOF spectrum (Fig. 1), intact parent dications were observed, suggesting that stable dications do exist. Photoion–photoion coincidence measurements of vinyl bromide reveal

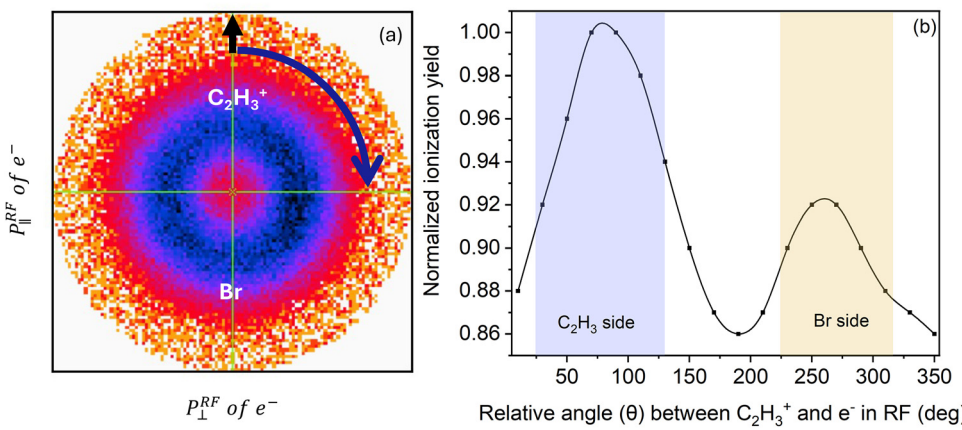

Fig. 3 (a) Recoil-frame electron momentum distribution for dissociative single ionization of vinyl bromide leading to the production of $C_2H_3^+$and Br. The black arrow indicates that the $C_2H_3^+$ recoil momentum is fixed upward while the blue arrow shows rotation direction of the electric field (helicity of the circularly polarized light). (b) Angle-dependent ionization yield for dissociative single ionization in vinyl bromide.

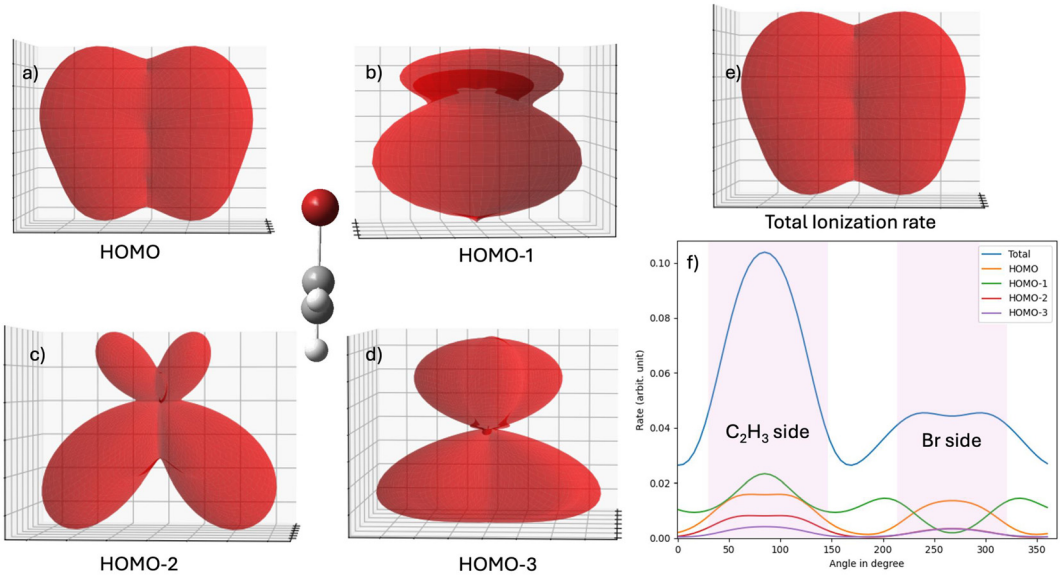

Fig. 4 Simulated ionization rates corresponding to the cationic states that contribute to the dissociative ionization channels of vinyl bromide. (a)–(d) The three-dimensional angular distributions of the calculated strong-field ionization rate associated with the HOMO, HOMO−1, HOMO−2, and HOMO−3 orbitals, respectively. (e) The total ionization rate obtained from simulation. (f) The orientation-averaged ionization rates as a function of angle along the C–Br bond axis, highlighting contributions from the vinyl (C_2H_3) side and the bromine side. The molecular structure of vinyl bromide defining the C–Br axis is shown as an inset.

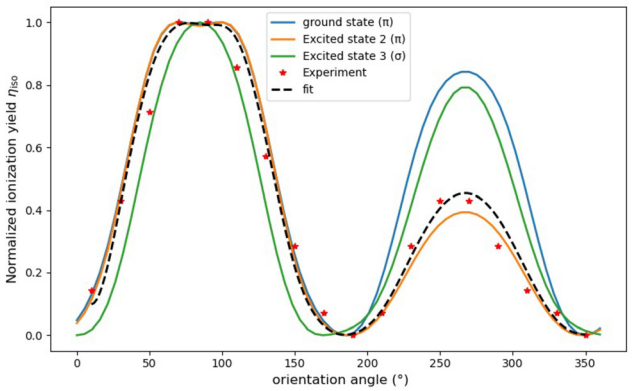

Fig. 5 Comparison of the experimental angle dependent ionization yield η_{iso} (red star markers) with the simulated ionization yields corresponding to the π-type (blue and orange lines) and σ-type (green line) excited states of the vinyl bromide cation. The experimental data were fitted using 85% contribution from HOMO−2 and 15% contribution from HOMO−3 (black dashed line).

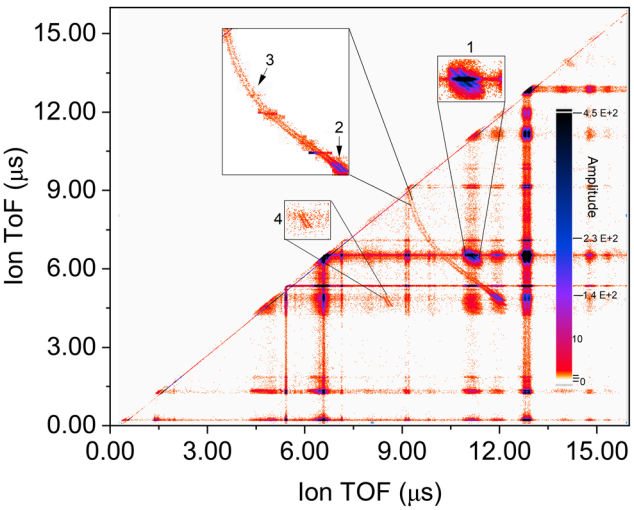

Fig. 6 Photoion–photoion coincidence (PIPICO) map of dissociative double/triple ionization of vinyl bromide with various channels isolated and labeled as insets: (1) the $C_2H_3^+$ + Br^+ channel; (2) the prompt CH_3^+ + CBr^+ channel; (3) the metastable CH_3^+ + CBr^+ channel; and (4) the minor dissociative triple ionization channel CH_2^+ + CBr^{2+} + H.

three dominant dissociation channels following double ionization (Fig. 6). The first channel is C–Br bond breaking, producing $C_2H_3^+$ + Br^+ ions with a small TOF extension (feature 1 in Fig. 6). Three distinct peaks appear in this channel due to bromine isotopes ($C_2H_3^+$ + $^{79}Br^+$, $C_2H_3^+$ + $^{81}Br^+$, and $C_2H_2^+$ + $H^{79}Br^+$). The compact TOF feature suggests that the dication is short-lived (a few nanoseconds or faster). The second dissociation channel yields the CH_3^+ + CBr^+ fragment *via* C=C bond cleavage, also from short-lived dications (feature 2 in Fig. 6). Here, bromine isotopes produce two separate lines: CH_3^+ + $C^{79}Br^+$ and CH_3^+ + $C^{81}Br^+$. A third channel is the diffusive feature with an extended TOF range (feature 3 in Fig. 6). This connects to the prompt channel of CH_3^+ + CBr^+, which suggests that it still arises from C=C bond breakage. However, the large TOF ranges indicate metastable dication states with a lifetime comparable to the TOF of the fragments, which amounts to a few microseconds. What are the origins of these dissociation channels? To answer this question, the energetics of key

species/states along different dissociation pathways on both the singlet and triplet potential energy surfaces were computed using high-level electronic structure methods, and the results are shown in Fig. 7. The relative enthalpies at 0 K were computed at the CBS-QB3 level. The B3LYP/6-311++G(3d,2p) energies are shown for comparison. CCSD/cc-pVTZ energies are also listed in Tables S1–S3 of the SI. In general, the energies agree to an average of 0.3 eV, with the CBS-QB3 values being the most reliable. Vertical double ionization energy to the singlet is 27.31 eV and removes 2 electrons from the π HOMO. This structure rotates 90° about the C–C bond to relax to a structure that is 1.02 eV lower in energy, which is taken as the reference energy for the other structures on the energy surface. Vertical double ionization to the triplet requires 27.65 eV and removes one electron from the π HOMO and one electron from a σ lone pair on bromine. The triplet dication relaxes to a planar structure that is 0.31 eV lower. Excited states of the vertically ionized singlet and triplet dications were also calculated at the CASPT2(10,10)/cc-pVTZ level. If excited states contribute to any dissociation pathways, fast internal conversion is expected to take place before the dynamics on the ground state surfaces.

The two main pathways for fragmentation on both the singlet and triplet surfaces are dissociation of the C–Br bond and dissociation of the C–C bond, preceded by hydrogen migration. We will first discuss the C–Br bond breakage channel. On the singlet surface, C-Br dissociation has a barrier of 2.53 eV (TS4) from the adiabatically ionized dication. The products of dissociation are singlet $C_2H_3^+$ and singlet Br^+. The high barrier suggests the two lowest singlet states (S0 and S1) cannot contribute to the observed $C_2H_3^+ + Br^+$ channel. Only excited singlet states such as S2 can produce this dissociation channel. However, the barrier for C–Br dissociation on the triplet surface is lower at 0.85 eV (TS2) from the relaxed triplet vinyl bromide dication. Energetically, excited states such as T1 have enough energy to produce the dissociation channel. We note a significant energy difference (~0.71 eV) in the reverse barrier height between the singlet and triplet transition states (TS4 3.38 eV *vs.* TS2 4.09 eV). This suggests we should be able to identify the actual pathway (singlet *vs.* triplet) if we look at the translational energy release of fragments. Indeed, the measured translational energy is about 4.5 eV (Fig. 8), which is much closer to the reverse barrier of the triplet transition state. This unambiguously determines that triplet excited states are the dominant pathway for the observed prompt C–Br bond breaking channel. Singlet excited states (S2 and above) might still contribute, but their higher ionization potentials suggest the contribution is likely to be low. We can also conclude that the ground triplet state T0 is a significant source of the observed non-dissociative dication since the energy is significantly below that of both transition states (TS2 and TS3).

Dissociation of the C–C bond proceeds in two steps. First, the hydrogen migrates from the CHBr group to the CH_2 group. The barrier (TS1) is only 0.19 eV on the singlet surface because the hydrogen is already perpendicular to the H_2CC framework. The intermediate CH_3–CBr dication is 0.54 eV lower than the singlet vinyl bromide dication and still has a strong C–C bond with a length of 1.36 Å. To break this bond, 1.74 eV (TS6) is required from the intermediate, leading to singlet CH_3^+ and singlet CBr^+. The latter has a particularly stable electronic structure because it is isoelectronic with CO. The barrier for hydrogen migration on the triplet surface, 1.75 eV (TS3), is much higher than that on the singlet surface because significant geometric and electronic rearrangements are needed to reach the intermediate. The intermediate (Int_2) has a bent structure similar to that of a triplet carbene. Dissociation of the C–C bond has a barrier of 1.87 eV (TS5) and leads to singlet CH_3^+ and triplet CBr^+. The latter is 2.18 eV higher than singlet CBr^+, in line with the high singlet–triplet gap in the

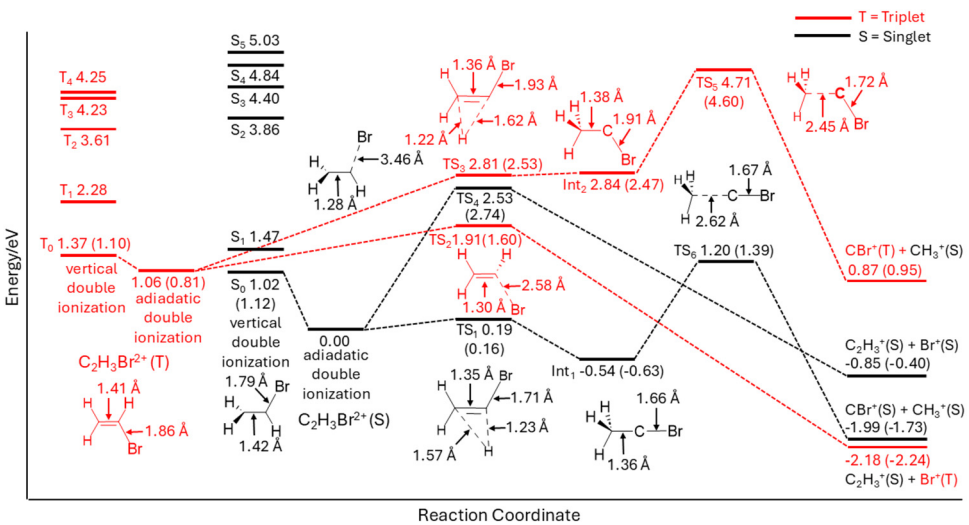

Fig. 7 Various dissociative double ionization pathways for vinyl bromide. The red and black color lines represent the triplet and singlets states of the dication, respectively. The bond distance of the molecular structures is denoted in Å. Energies (in eV) are reported at the CBS-QB3 level relative to the singlet $C_2H_3Br^{2+}$ minimum, with B3LYP/6-311G++(3d,2p) relative energies given in parentheses. Excitation energies were calculated at the MS-CASPT2(10,10)/cc-pVTZ level.

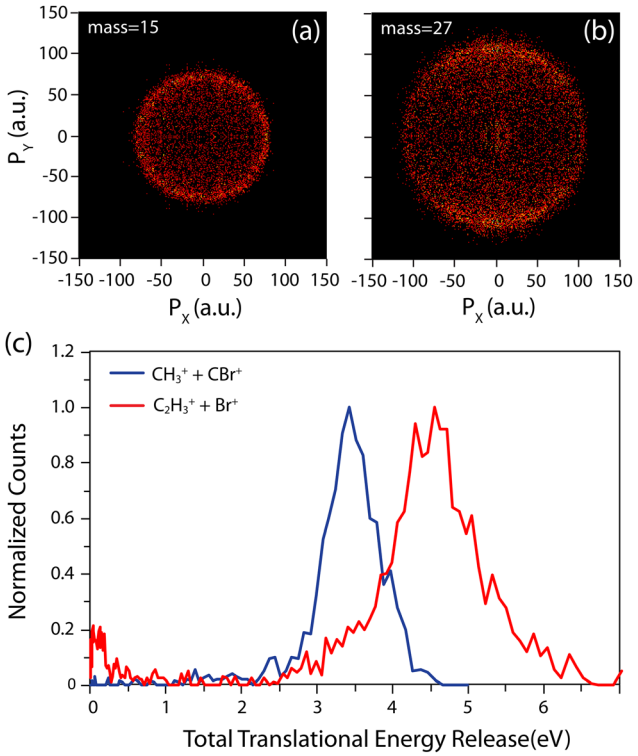

Fig. 8 Ion momentum distributions and the corresponding translational energy release (TER) spectra for the major dissociation channels: (a) CH_3^+ momentum distribution, (b) total TER for the CH_3^+ + CBr^+ channel, with a peak around 3.5 eV, (c) $C_2H_3^+$ momentum distribution, (d) total TER for $C_2H_3^+$ + Br^+ channel, with a peak at approximately 4.5 eV. Momentum calibration was performed using the known total TER distribution of the CH_3^+ + I^+ channel from the dissociative double ionization of methyl iodide.

isoelectronic CO. The two high barriers and the fact that even the most energetic dication triplet state (T4) lies below the transition state (TS5), effectively rule out the participation of the triplet surface in the C–C bond-breaking channel observed in the experiment. How about the singlet states? The excited singlet state S2 has enough energy to produce the prompt dissociative channel, but its yield is low due to its high ionization energy. Therefore, it is not likely to be the main source of the prompt C–C breaking channel. This leaves us just S0 and S1 states to consider. Interestingly, the energies of these states are very close to that of the transition state (TS6): one is 0.27 eV above, and one is 0.18 eV below. We can estimate the lifetime of the S1 state using the microcanonical transition state theory. We calculated the sum of state and density of state using the Beyer–Swinehart algorithm.[48] The vibrational frequencies of the intermediate (Int_1) and the transition state (TS6) are listed in the SI (see Tables S6 and S7). The small barrier for hydrogen migration (TS1) should not alter the overall rate, and thus, we focus on the rate constant for Int_1 dissociation. The calculated lifetime is 120 picoseconds at an excess energy of 0.27 eV for S1, which suggests that this will show up in the PIPICO spectrum as prompt dissociation. In principle, because the S0 state lies below the transition state, no reaction can take place. However, because the Franck–Condon region from the neutral vinyl bromide has a finite width, the energy of the S0 state should have a distribution reflecting the width of the ground vibrational state. Because the energy is so close to that of the transition state, the rate constant can vary dramatically with small energy differences. However, the calculation showed that even at the lowest excess energy, the computed rate constant exceeds 4.08×10^7 s^{-1}, which corresponds to a lifetime of ~25 ns. This lifetime is still too fast to be considered as metastable dications as observed in the experiment (measured lifetime: a few μs). A potential mechanism is a slow intersystem crossing (ISC) that converts triplet T0 and T1 into singlet states. Energetically, both states can dissociate promptly on the singlet surface to the CH_3^+ + CBr^+ channel. However, if the intersystem crossing is slow, it becomes the rate-limiting step and dictates the lifetime of the dissociation channel. We note that such a mechanism is also consistent with the absence of metastability in the $C_2H_3^+$ + Br^+ channel, because neither T0 nor T1 has enough energy on the singlet surface to overcome the dissociation barrier (TS4). To the best of our knowledge, there have been no reports on the timescale of intersystem crossing in vinyl bromide dications. Modeling such dynamics is beyond the scope of this work and will be explored in a future study.

Conclusion

The current study combines PIPICO measurements with recoil-frame photoelectron angular distributions and high-level electronic structure calculations to investigate the strong field ionization/dissociation dynamics of vinyl bromide. We showed that few-cycle pulses can suppress post-ionization excitation in vinyl bromide and thus simplify interpretations. Our results revealed that dissociative single ionization arises mainly from ionizing the HOMO−2 orbital. Detailed investigation into the dissociation pathways of vinyl bromide dications identifies contributions from both triplet and singlet states as well as ground and excited states. Furthermore, calculations showed that vinyl bromide dictations dissociate promptly on both the singlet and the triplet surfaces. We suggest that a slow intersystem crossing might be able to explain the observed metastability of dications that dissociate *via* hydrogen migration.

Conflicts of interest

There are no conflicts to declare.

Data availability

The data supporting this article have been included as part of the supplementary information (SI). Supplementary information includes computed relative energies of vinyl bromide cationic states and vibrational frequencies of key intermediates and transition states along reaction pathways. See DOI: https://doi.org/10.1039/d6cp00500d.

Acknowledgements

This research study was supported by the U.S. Department of Energy (DOE), Office of Science, Basic Energy Sciences (BES), under Award # DE-SC0020994. We thank Prof. Arthur Suits for the helpful discussion.

References

1 G. Basnayake, Y. Ranathunga, S. K. Lee and W. Li, Three-dimensional (3D) velocity map imaging: from technique to application, *J. Phys. B: At., Mol. Opt. Phys.*, 2022, **55**(2), 023001, DOI: 10.1088/1361-6455/ac4b42.

2 L. Fan, S. K. Lee, Y. J. Tu, B. Mignolet, D. Couch, K. Dorney, Q. Nguyen, L. Wooldridge, M. Murnane and F. Remacle, *et al.*, A new electron-ion coincidence 3D momentum-imaging method and its application in probing strong field dynamics of 2-phenylethyl-*N*,*N*-dimethylamine, *J. Chem. Phys.*, 2017, **147**(1), 013920, DOI: 10.1063/1.4981526.

3 J. Ullrich, R. Moshammer, A. Dorn, R. Dörner, L. P. H. Schmidt and H. Schmidt-Böcking, Recoil-ion and electron momentum spectroscopy: reaction-microscopes, *Rep. Prog. Phys.*, 2003, **66**(9), 1463–1545, DOI: 10.1088/0034-4885/66/9/203.

4 C. Wu, Z. Wu, Q. Liang, M. Liu, Y. Deng and Q. Gong, Ionization and dissociation of alkanes in few-cycle laser fields, *Phys. Rev. A*, 2007, **75**(4), 043408, DOI: 10.1103/PhysRevA.75.043408.

5 L. Varvarezos, J. T. Costello, C. Long, A. J. Achner, R. Wagner, M. Meyer and P. Grychtol, Ionization–dissociation of methane in ultrashort 400 nm and 800 nm laser fields, *Chem. Phys. Lett.*, 2021, **775**, 138687, DOI: 10.1016/j.cplett.2021.138687.

6 A. E. Boguslavskiy, J. Mikosch, A. Gijsbertsen, M. Spanner, S. Patchkovskii, N. Gador, M. J. J. Vrakking and A. Stolow, The Multielectron Ionization Dynamics Underlying Attosecond Strong-Field Spectroscopies, *Science*, 2012, **335**(6074), 1336–1340, DOI: 10.1126/science.1212896.

7 J. Mikosch, A. E. Boguslavskiy, I. Wilkinson, M. Spanner, S. Patchkovskii and A. Stolow, Channel- and Angle-Resolved Above Threshold Ionization in the Molecular Frame, *Phys. Rev. Lett.*, 2013, **110**(2), 023004.

8 H. Akagi, T. Otobe, A. Staudte, A. Shiner, F. Turner, R. Dörner, D. M. Villeneuve and P. B. Corkum, Laser Tunnel Ionization from Multiple Orbitals in HCl, *Science*, 2009, **325**(5946), 1364–1367, DOI: 10.1126/science.1175253.

9 J. Wu, M. Magrakvelidze, L. P. H. Schmidt, M. Kunitski, T. Pfeifer, M. Schöffler, M. Pitzer, M. Richter, S. Voss and H. Sann, Understanding the role of phase in chemical bond breaking with coincidence angular streaking, *Nat. Commun.*, 2013, **4**(1), 2177.

10 A. H. Winney, G. Basnayake, D. A. Debrah, Y. F. Lin, S. K. Lee, P. Hoerner, Q. Liao, H. B. Schlegel and W. Li, Disentangling Strong-Field Multielectron Dynamics with Angular Streaking, *J. Phys. Chem. Lett.*, 2018, **9**, 2539–2545, DOI: 10.1021/acs.jpclett.8b00028.

11 D. Pavicic, K. F. Lee, D. M. Rayner, P. B. Corkum and D. M. Villeneuve, Direct measurement of the angular dependence of ionization for N-2, O-2, and CO_2 in intense laser fields, *Phys. Rev. Lett.*, 2007, **98**(24), 243001, DOI: 10.1103/PhysRevLett.98.243001.

12 I. Thomann, R. Lock, V. Sharma, E. Gagnon, S. T. Pratt, H. C. Kapteyn, M. M. Murnane and W. Li, Direct measurement of the angular dependence of the single-photon ionization of aligned N_2 and CO_2, *J. Phys. Chem. A*, 2008, **112**(39), 9382–9386, DOI: 10.1021/jp8023414.

13 R. E. Continetti, Coincidence Spectroscopy, *Annu. Rev. Phys. Chem.*, 2001, **52**, 165–192, DOI: 10.1146/annurev.physchem.52.1.165.

14 M. Lee and M. S. Kim, Mass-analyzed threshold ionization study of vinyl bromide cation in the first excited electronic state using vacuum-ultraviolet radiation generated by four-wave mixing in Hg, *J. Chem. Phys.*, 2005, **123**(17), 174310, DOI: 10.1063/1.2104530.

15 M. Lee and M. S. Kim, Photodissociation yield spectroscopy of vinyl bromide cation generated by mass-analyzed threshold ionization: Vibrational spectroscopy and decay dynamics in the B̃ state, *J. Chem. Phys.*, 2007, **126**(15), 154317, DOI: 10.1063/1.2721541.

16 M. Lee and M. S. Kim, Vacuum ultraviolet mass-analyzed threshold ionization spectroscopy of vinyl bromide: Franck–Condon analysis and vibrational assignment, *J. Chem. Phys.*, 2003, **119**(10), 5085–5093, DOI: 10.1063/1.1597493.

17 M. Yamaguchi, Multireference Configuration Interaction Study of the Vibronic Transitions and Photodissociation of Vinyl Bromide and Vinyl Chloride Radical Cations in the Second Excited State, *J. Phys. Chem. A*, 2010, **114**(30), 7937–7944, DOI: 10.1021/jp9121722.

18 M.-F. Lin, D. M. Neumark, O. Gessner and S. R. Leone, Ionization and dissociation dynamics of vinyl bromide probed by femtosecond extreme ultraviolet transient absorption spectroscopy, *J. Chem. Phys.*, 2014, **140**(6), 064311, DOI: 10.1063/1.4865128.

19 L.-X. Zhou, Y. Liu, S. He, D.-S. Gao, X.-C. Shen, Q. Chen, T. Yu, H. Lv and H.-F. Xu, Ultrafast dynamics of cationic electronic states of vinyl bromide by strong-field ionization-photofragmentation, *Chin. Phys. B*, 2022, **31**(2), 028202, DOI: 10.1088/1674-1056/ac2b15.

20 F. Rott, M. Reduzzi, T. Schnappinger, Y. Kobayashi, K. F. Chang, H. Timmers, D. M. Neumark, R. D. Vivie-Riedle and S. R. Leone, Ultrafast strong-field dissociation of vinyl bromide: An attosecond transient absorption spectroscopy and non-adiabatic molecular dynamics study, *Struct. Dyn.*, 2021, **8**(3), 034104, DOI: 10.1063/4.0000102.

21 M. Castillejo, M. Martín, R. de Nalda, S. Couris and E. Koudoumas, Anisotropic Distributions of Ion Fragments Produced by Dissociative Ionization of Halogenated Ethylenes in Intense Laser Fields, *J. Phys. Chem. A*, 2002, **106**(12), 2838–2843, DOI: 10.1021/jp013446q.

22 Y. Liu, S. He, L. Zhou, Q. Chen, Y. Zhao, T. Sun, X. Shen, T. Yu, H. Lv and H. Xu, Strong-field photoionization/dissociation of vinyl bromide in near-infrared and ultraviolet

femtosecond laser fields, *J. Opt. Soc. Am. B*, 2023, **40**(7), 1851–1856, DOI: 10.1364/JOSAB.489934.

23 X. M. Qian, K. C. Lau and C. Y. Ng, A high-resolution pulsed field ionization-photoelectron-photoion coincidence study of vinyl bromide, *J. Chem. Phys.*, 2004, **120**(23), 11031–11041, DOI: 10.1063/1.1739402.

24 H. Du, C. Covington, S. R. Leone and K. Varga, Excited-state electronic coherence in vinyl bromide ions, *Phys. Rev. A*, 2019, **100**(5), 053412, DOI: 10.1103/PhysRevA.100.053412.

25 S. K. Lee, F. Cudry, Y. F. Lin, S. Lingenfelter, A. H. Winney, L. Fan and W. Li, Coincidence ion imaging with a fast frame camera, *Rev. Sci. Instrum.*, 2014, **85**(12), 123303, DOI: 10.1063/1.4903856.

26 M. Miranda, C. L. Arnold, T. Fordell, F. Silva, B. Alonso, R. Weigand, A. L'Huillier and H. Crespo, Characterization of broadband few-cycle laser pulses with the d-scan technique, *Opt. Express*, 2012, **20**(17), 18732–18743, DOI: 10.1364/OE.20.018732.

27 G. A. Stewart, P. Hoerner, D. A. Debrah, S. K. Lee, H. B. Schlegel and W. Li, Attosecond Imaging of Electronic Wave Packets, *Phys. Rev. Lett.*, 2023, **130**(8), 083202, DOI: 10.1103/PhysRevLett.130.083202.

28 D. A. Debrah, G. A. Stewart, G. Basnayake, J. W. G. Tisch, S. K. Lee and W. Li, Direct in-situ single-shot measurements of the absolute carrier-envelope phases of ultrashort pulses, *Opt. Lett.*, 2019, **44**(14), 3582–3585, DOI: 10.1364/OL.44.003582.

29 G. Basnayake, P. Hoerner, B. Mignolet, M. K. Lee, Y. F. Lin, A. H. Winney, D. A. Debrah, L. Popaj, X. Shi and S. K. Lee, *et al.*, Ellipticity controlled dissociative double ionization of ethane by strong fields, *Phys. Chem. Chem. Phys.*, 2021, **23**(41), 23537–23543, DOI: 10.1039/D1CP03585A.

30 M. J. Frisch, G. W. Trucks, H. B. Schlegel, G. E. Scuseria, M. A. Robb, J. R. Cheeseman, G. Scalmani, V. Barone, G. A. Petersson, H. Nakatsuji, *et al.*, *Gaussian 16, Revision A.03*, Gaussian, Inc., Wallingford, CT, 2016.

31 A. D. Becke, Density-functional exchange-energy approximation with correct asymptotic behavior, *Phys. Rev. A: At., Mol., Opt. Phys.*, 1988, **38**(6), 3098–3100, DOI: 10.1103/PhysRevA.38.3098.

32 A. D. Becke, Density-functional thermochemistry. III. The role of exact exchange, *J. Chem. Phys.*, 1993, **98**(7), 5648–5652, DOI: 10.1063/1.464913.

33 R. Krishnan, J. S. Binkley, R. Seeger and J. A. Pople, Self-consistent molecular orbital methods. XX. A basis set for correlated wave functions, *J. Chem. Phys.*, 1980, **72**(1), 650–654, DOI: 10.1063/1.438955.

34 T. H. Dunning Jr., Gaussian basis sets for use in correlated molecular calculations. I. The atoms boron through neon and hydrogen, *J. Chem. Phys.*, 1989, **90**(2), 1007–1023, DOI: 10.1063/1.456153.

35 A. C. Scheiner, G. E. Scuseria, J. E. Rice, T. J. Lee and H. F. Schaefer III, Analytic evaluation of energy gradients for the single and double excitation coupled cluster (CCSD) wave function: Theory and application, *J. Chem. Phys.*, 1987, **87**(9), 5361–5373, DOI: 10.1063/1.453655.

36 M. R. Nyden and G. A. Petersson, Complete basis set correlation energies. I. The asymptotic convergence of pair natural orbital expansions, *J. Chem. Phys.*, 1981, **75**(4), 1843–1862, DOI: 10.1063/1.442208.

37 G. A. Petersson and M. A. Al-Laham, A complete basis set model chemistry. II. Open-shell systems and the total energies of the first-row atoms, *J. Chem. Phys.*, 1991, **94**(9), 6081–6090, DOI: 10.1063/1.460447.

38 G. A. Petersson, T. G. Tensfeldt and J. A. Montgomery Jr., A complete basis set model chemistry. III. The complete basis set-quadratic configuration interaction family of methods, *J. Chem. Phys.*, 1991, **94**(9), 6091–6101, DOI: 10.1063/1.460448.

39 J. A. Montgomery Jr., J. W. Ochterski and G. A. Petersson, A complete basis set model chemistry. IV. An improved atomic pair natural orbital method, *J. Chem. Phys.*, 1994, **101**(7), 5900–5909, DOI: 10.1063/1.467306.

40 H. P. Hratchian and H. B. Schlegel, Accurate reaction paths using a Hessian based predictor–corrector integrator, *J. Chem. Phys.*, 2004, **120**(21), 9918–9924, DOI: 10.1063/1.1724823.

41 B. O. Roos, P. R. Taylor and P. E. M. Sigbahn, A complete active space SCF method (CASSCF) using a density matrix formulated super-CI approach, *Chem. Phys.*, 1980, **48**(2), 157–173, DOI: 10.1016/0301-0104(80)80045-0.

42 K. Andersson, P. Å. Malmqvist and B. O. Roos, Second-order perturbation theory with a complete active space self-consistent field reference function, *J. Chem. Phys.*, 1992, **96**(2), 1218–1226, DOI: 10.1063/1.462209.

43 C. Melania Oana and A. I. Krylov, Dyson orbitals for ionization from the ground and electronically excited states within equation-of-motion coupled-cluster formalism: Theory, implementation, and examples, *J. Chem. Phys.*, 2007, **127**(23), 234106, DOI: 10.1063/1.2805393.

44 P. Hoerner and H. B. Schlegel, Angular Dependence of Strong Field Ionization of Haloacetylenes HCCX (X = F, Cl, Br, I), Using Time-Dependent Configuration Interaction with an Absorbing Potential, *J. Phys. Chem. C*, 2018, **122**(25), 13751–13757, DOI: 10.1021/acs.jpcc.8b00619.

45 A. S. Durden and H. B. Schlegel, Reducing the Cost of TD-CI Simulations of Strong Field Ionization, *J. Phys. Chem. A*, 2024, **128**(35), 7440–7450, DOI: 10.1021/acs.jpca.4c01732.

46 A. S. Durden and H. B. Schlegel, Evaluation of Diffuse Basis Sets for Simulations of Strong Field Ionization Using Time-Dependent Configuration Interaction with a Complex Absorbing Potential, *J. Phys. Chem. A*, 2025, **129**(14), 3353–3367, DOI: 10.1021/acs.jpca.5c00195.

47 M. Lee and M. S. Kim, Vibrational Spectroscopy and State-Specific Dissociation Dynamics for Vinyl Chloride Cation in the B̃ State, *J. Phys. Chem. A*, 2007, **111**(34), 8409–8415, DOI: 10.1021/jp0718810.

48 T. Beyer and D. F. Swinehart, Algorithm 448: number of multiply-restricted partitions, *Commun. ACM*, 1973, **16**(6), 379, DOI: 10.1145/362248.362275.